

Linear Sensitivity of Helioseismic Travel Times to Local Flows

A.C. Birch^{1,*} and L. Gizon²

¹ NWRA, CoRA Division, 3380 Mitchell Lane, Boulder CO 80301 USA

² Max-Planck-Institut für Sonnensystemforschung, Max-Planck-Straße 2, 37191 Katlenburg-Lindau, Germany

Received 30 May 2005, accepted 11 Nov 2005

Published online later

Key words Sun:helioseismology – Sun:interior – scattering

Time-distance helioseismology is a technique for measuring the time for waves to travel from one point on the solar surface to another. These wave travel times are affected by advection by subsurface flows. Inferences of plasma flows based on observed travel times depend critically on the ability to accurately model the effects of subsurface flows on time-distance measurements. We present a Born-approximation based computation of the sensitivity of time-distance travel times to weak, steady, inhomogeneous subsurface flows. Three sensitivity functions are obtained, one for each component of the 3D vector flow. We show that the depth sensitivity of travel times to horizontally uniform flows is given approximately by the kinetic energy density of the oscillation modes which contribute to the travel times. For flows with strong depth dependence, the Born approximation can give substantially different results than the ray approximation.

© 2007 WILEY-VCH Verlag GmbH & Co. KGaA, Weinheim

1 Introduction

Time-distance helioseismology (Duvall et al. 1993) is a technique for measuring the time for waves to travel from one point on the solar surface to another. Subsurface flows advect waves and as a result alter the observed travel times. Thus wave travel times can be used as probes of subsurface flows (e.g. Kosovichev & Duvall 1997, Zhao et al. 2004)

One of the key steps in the interpretation of travel times is to estimate the effect of subsurface flows on travel times. The ray approximation (Kosovichev & Duvall 1997), in which travel-time shifts are only caused by inhomogeneities located along the ray path connecting the observation points, has been employed in many time-distance studies of plasma flows (e.g. Kosovichev & Duvall 1997, Zhao et al. 2001, Zhao & Kosovichev 2003, Zhao et al. 2004). An alternative to the ray approximation is the first Born approximation (e.g. Birch & Kosovichev 2000; Gizon & Birch 2002, in the context of time-distance helioseismology). The first Born approximation takes into account a single scattering and thus flows located away from the ray path can affect the travel time.

Birch & Felder (2004) studied the ranges of validity of the Born and ray approximations in a toy problem consisting of jets in a homogeneous two-dimensional medium. This study showed that there are flow configurations for which the Born approximation is valid while the ray approximation is not, especially when the transverse size of the jet is much smaller than the wavelength. As a result, we would like to use the first Born approximation to compute the sen-

sitivity of travel times to flows for use in time-distance helioseismology.

Here we employ the Born approximation approach of Gizon & Birch (2002), referred to as GB02 hereafter, to compute the sensitivity of travel times to weak, steady, three-dimensional subsurface flows in the Sun. We use the phenomenological model of Birch et al. (2004), referred to as B04 hereafter, to describe how waves are excited and damped by convection. We work in Cartesian geometry, which is appropriate for waves that travel distances much less than the solar radius and also have wavelengths much smaller than the solar radius.

The remainder of this paper is organized as follows. In §2 we derive the general expression for the sensitivity of travel times to weak flows. In §3 we show a few example calculations. We compare the Born and ray approximations in §4. We conclude in §5 with a summary and a short discussion of the implications of the work presented here.

2 Sensitivity Functions

In this section we use the Born approximation to obtain the linear sensitivity of travel times to weak and steady subsurface flows. We are looking for kernels $\mathbf{K} = (K_x, K_y, K_z)$ which satisfy

$$\delta\tau(\mathbf{x}_1, \mathbf{x}_2) = \iiint_{\odot} d\mathbf{r} \mathbf{K}(\mathbf{r}; \mathbf{x}_1, \mathbf{x}_2) \cdot \mathbf{v}(\mathbf{r}), \quad (1)$$

where the integration variable \mathbf{r} runs over the entire volume of the solar model and $\mathbf{v} = (v_x, v_y, v_z)$ is the flow field. Throughout this paper we will denote three-dimensional position vectors by $\mathbf{r} = (x, z)$ where $\mathbf{x} = (x, y)$ is the horizontal position vector and z is depth. The travel-time dif-

* Corresponding author: e-mail: aaronb@cora.nwra.com

ference between surface locations \mathbf{x}_1 and \mathbf{x}_2 is denoted as $\delta\tau(\mathbf{x}_1, \mathbf{x}_2)$ and defined by

$$\delta\tau(\mathbf{x}_1, \mathbf{x}_2) = \tau_+(\mathbf{x}_1, \mathbf{x}_2) - \tau_+(\mathbf{x}_2, \mathbf{x}_1), \quad (2)$$

where $\tau_+(\mathbf{x}_i, \mathbf{x}_j)$ is the one-way travel time, as defined by GB02, from \mathbf{x}_i to \mathbf{x}_j .

Following GB02 and B04, we begin by considering damped and driven solar oscillations with a displacement field ξ that obeys, to lowest order in the flow velocity \mathbf{v} ,

$$[\mathcal{L}_0 + \delta\mathcal{L}]\xi = \mathbf{S}, \quad (3)$$

with the wave equation operator in the absence of flows, \mathcal{L}_0 (e.g. Lynden-Bell & Ostriker 1967), given by

$$\mathcal{L}_0\xi = \rho_0\ddot{\xi} - \nabla[\gamma p_0\nabla\cdot\xi + \xi\cdot\nabla p_0] + (\nabla\cdot\xi)\nabla p_0 + \xi\cdot\nabla(\nabla p_0) + \rho_0\partial_t(\Gamma\xi), \quad (4)$$

where ρ_0 , p_0 , and γ are the background density, pressure, and ratio of specific heats. We use solar model S (Christensen-Dalsgaard et al. 1996). The damping operator is Γ (B04). In equation (4) we have used the Cowling approximation and also neglected the variation of the gravitational acceleration with depth. We have also neglected the Coriolis force. The source function \mathbf{S} is intended to represent the driving of oscillations by near-surface turbulent convection. In order to compute the covariance of the wavefield ξ we only need the covariance of the source \mathbf{S} . We choose to use the source covariance described by B04.

The first-order perturbation to the wave equation introduced by a flow (e.g. Lynden-Bell & Ostriker 1967) is given by

$$\delta\mathcal{L}\xi = 2\rho_0\partial_t\mathbf{v}\cdot\nabla\xi. \quad (5)$$

This term only captures the direct advection of waves by the flow \mathbf{v} . Any associated changes in the background (non-wave) density and sound speed are neglected. The problem of the sensitivity of travel-times to changes in sound speed has already been addressed by B04. Density perturbations could be treated in essentially the same manner.

The observations used for time-distance helioseismology are typically time series of images of the line-of-sight Doppler velocity near the solar surface. For the sake of simplicity we assume that the line-of-sight is vertical. In addition, we approximate the Doppler velocity as the time derivative of the displacement at a fixed geometrical height $z_{\text{obs}} = 200$ km. In this case, the observed wavefield, $\phi(\mathbf{x}, t)$, is related to the wave displacement by

$$\phi(\mathbf{x}, t) = \mathcal{F}\{\partial_t\xi_z(\mathbf{x}, t, z_{\text{obs}})\}, \quad (6)$$

where the function \mathcal{F} denotes the action of the instrument point-spread function and any filters applied during the data analysis (e.g. phase-speed filters). In the Fourier domain, we can write the wavefield as

$$\phi(\mathbf{k}, \omega) = -i\omega F(\mathbf{k}, \omega)\xi_z(\mathbf{k}, \omega, z_{\text{obs}}), \quad (7)$$

where \mathbf{k} is the horizontal wavevector, ω the angular frequency, and $F(\mathbf{k}, \omega)$ represents the filter in the Fourier domain. Throughout this paper we will employ the Fourier

convention of GB02, for a function f of horizontal position and time, we have

$$f(\mathbf{x}, t) = \int d\mathbf{k}d\omega f(\mathbf{k}, \omega)e^{i\mathbf{k}\cdot\mathbf{x}-i\omega t}. \quad (8)$$

We will employ the same symbol for functions and their Fourier transforms, e.g. $f(\mathbf{k}, \omega)$ denotes the transform of $f(\mathbf{x}, t)$.

In order to compute travel-time kernels we need first to obtain Green's functions. We define Green's functions \mathbf{G}^j as the solutions to

$$\mathcal{L}^0\mathbf{G}^j(\mathbf{x}, t, z, z') = \hat{\mathbf{e}}_j\delta(\mathbf{x})\delta(t)\delta(z-z'), \quad (9)$$

where $\hat{\mathbf{e}}_j$ with $j = x, y, z$ are unit vectors along the coordinate axes. We use the same boundary conditions as in B04: zero Lagrangian pressure at the top of model S and no vertical motion at a depth of 300 Mm below the photosphere (this bottom boundary condition has essentially no effect on the computations presented here). The Green's vector $\mathbf{G}^j(\mathbf{x}, t, z, z')$ gives the displacement response as a function of horizontal position \mathbf{x} , time t , and height z , to a delta function source in the $\hat{\mathbf{e}}_j$ direction at horizontal position $\mathbf{0}$, time $t = 0$, and height z' . We use the normal-mode summation approximation solution to equation (9) given by B04.

We now have all of the ingredients to compute travel-time kernels using the recipe of equations (26) and (32) from GB02. The result for the kernels for velocity is

$$K_j(\mathbf{r}; \mathbf{x}_1, \mathbf{x}_2) = 4\pi\text{Re}\int_0^\infty d\omega W_{\text{diff}}^*(\omega)\mathcal{C}_j(\mathbf{r}; \mathbf{x}_2|\mathbf{x}_1; \omega), \quad (10)$$

with $j = x, y, z$. The function W_{diff} is the linear sensitivity of the travel-time to changes in the cross-covariance and is defined in GB02. The sensitivity of the cross-covariance to flows in the j direction is denoted by \mathcal{C}^j and given by

$$\begin{aligned} \mathcal{C}_j(\mathbf{r}; \mathbf{x}_2|\mathbf{x}_1; \omega) &= 2(2\pi)^7 i\omega^3 \rho_0(z)m(\omega) \\ &\times [\mathbf{II}^j(\mathbf{x} - \mathbf{x}_1, z, \omega) \cdot \mathbf{I}(\mathbf{x} - \mathbf{x}_2, z, \omega) \\ &+ \mathbf{II}^{j*}(\mathbf{x} - \mathbf{x}_2, z, \omega) \cdot \mathbf{I}^*(\mathbf{x} - \mathbf{x}_1, z, \omega)]. \end{aligned} \quad (11)$$

where $\mathbf{r} = (\mathbf{x}, z)$. The function $m(\omega)$ is the source auto-correlation function defined in B04. The vectors $\mathbf{I}(\mathbf{x})$ and $\mathbf{II}(\mathbf{x})$ we define in terms of their horizontal Fourier transforms:

$$\mathbf{I}^j(\mathbf{k}, z, \omega) = F(-\mathbf{k}, \omega)G_z^j(-\mathbf{k}, \omega, z_{\text{obs}}, z), \quad (12)$$

$$\mathbf{II}^j(\mathbf{k}, z, \omega) = F(\mathbf{k}, \omega)H_z^*(\mathbf{k}, \omega, z_{\text{obs}})\partial_j\mathbf{H}^*(\mathbf{k}, \omega, z). \quad (13)$$

The Green's vector \mathbf{H} is defined as

$$\mathbf{H}(\mathbf{k}, \omega, z) = \partial_{z'}\mathbf{G}^z(\mathbf{k}, \omega, z, z')|_{z'=z_{\text{src}}}, \quad (14)$$

where the source depth z_{src} is chosen to be 100 km below the photosphere (see B04 for a discussion of the source model). The general mathematical structure of the kernels was explained by GB02.

3 Example Calculations

In this section we show the results of two example calculations. The first example is for p_1 travel-time differences for the travel distance $\Delta = \|\mathbf{x}_2 - \mathbf{x}_1\| = 7$ Mm obtained using a phase-speed filter. The second example is for surface gravity wave travel-time differences at a travel distance of $\Delta = 10$ Mm.

3.1 p_1 ridge

For the first example, the filter function $F(k, \omega)$ is given as the product of three separate filters,

$$F(\mathbf{k}, \omega) = F_1(k, \omega)F_2(k, \omega)\text{OTF}(k). \quad (15)$$

The filter F_1 removes the f -mode ridge and frequencies below 1.5 mHz and above 5 mHz. The phase-speed filter, F_2 , is given by

$$F_2(\mathbf{k}, \omega) = e^{-(\omega/k - v_p)^2 / 2\delta v_p^2}, \quad (16)$$

with $k = \|\mathbf{k}\|$, $v_p = 12.8$ km/s and $\delta v_p = 2.6$ km/s (this is filter 1 from Couvidat et al. 2006). This filter isolates a section of the p_1 ridge. Finally a filter $\text{OTF}(\mathbf{k}) = e^{-\alpha k}$ with $\alpha = 1.75$ Mm is used as a very rough approximation for the optical transfer function of the MDI/SOHO high-resolution observing mode.

Figure 1 shows slices through the components of the kernel \mathbf{K} for travel-time differences, for the p_1 case. Figure 1a shows a slice through K_x at the photosphere. This kernel is symmetric in both x and y . As with the kernels shown by GBO2 and B04, ellipse- and hyperbola-shaped features are visible. The ringing in the horizontal directions is a result of the finite band-width of the wavefield. Figures 1b and 1c show horizontal slices through the kernels K_y and K_z at the photosphere. Different symmetries are visible in these slices; K_y is anti-symmetric in both x and y , while K_z is symmetric in y and antisymmetric in x . Because of these symmetries both K_y and K_z integrate to zero. The kernel K_x has a non-zero total integral; spatially uniform flows in the \hat{x} direction cause travel-time differences.

Figure 1d shows a vertical slice through K_x at $y = 0$. Also shown is the ray path corresponding to a frequency of 4.5 mHz. The maximum height of the ray path is limited by the upper turning point (80 km below the photosphere). For small travel distances Δ , such as the example shown here, the lower turning point of the ray path is frequency dependent. In this case we have chosen to compute a ray at 4.5 mHz, which is the frequency where the wavefield has maximum power (after filtering). The p_1 mode structure is visible in K_x . There is one maximum in sensitivity near the photosphere, and another near the lower turning point of the mode. This depth dependence will be discussed in later in this section.

A slice through K_z at $y = 0$ is shown in Figure 1e. The kernel K_z is largest where the ray is mostly vertical, as expected from the ray approximation.

3.2 Surface gravity waves

For the second example we compute the sensitivity of f -mode travel-time differences to flow, for the case of a travel distance $\Delta = 10$ Mm. In this case the filter function F was chosen to be

$$F(k, \omega) = F_3(k, \omega)\text{OTF}(k) \quad (17)$$

The filter F_3 selects only the f -mode and removes all p -modes and frequencies below 1.5 mHz and above 5 mHz.

Figure 2 shows the results of the example f -mode calculation. The kernels K_x , K_y , and K_z show the same symmetries as in the p -mode case shown in Figure 1. As a result the kernel K_x has a non-zero total integral, while K_y and K_z both integrate to zero.

A horizontal slice at the photosphere through K_x is shown in Figure 2a. Notice that the K_x kernel is the three-dimensional version of the kernel shown by Gizon et al. (2000) and in more detail by Jackiewicz et al. (2006).

Figure 3 shows the depth dependence of the sensitivity functions shown in Figures 1 and 2, for the case of horizontally uniform flows. In both cases, the depth dependence is roughly proportional to the kinetic energy density of the associated mode. This assumption was suggested for the f -mode by Gizon & Duvall (2000b).

4 Comparison with Ray Theory

As described in the introduction, the ray approximation (Kosovichev & Duvall 1997) has been used to predict the travel-time shifts caused by sub-surface flows. In this section we compare the predictions of the ray and Born approximations. We will consider here very simple models of flows at supergranular scales. We choose to study cylindrically symmetric flow fields, $\mathbf{v}(r, z) = v_z(r, z)\hat{\mathbf{z}} + v_r(r, z)\hat{\mathbf{r}}$, of the form:

$$v_r(r, z) = af(r)h(z), \quad (18)$$

$$v_z(r, z) = \frac{a}{r}\partial_r [rf(r)]n(z), \quad (19)$$

where r is the distance from the symmetry axis of the flow and z is depth. The horizontal variation of the radial flow is given by

$$f(r) = J_0(kr)e^{-r/L}, \quad (20)$$

where L is the decay length of the flow away from the center of the cell, and k is the wavenumber associated with the radial variation in the flow. The depth variation of the radial velocity we choose as

$$h(z) = e^{-(z-z_t)^2/D_1^2} - \beta e^{-(z-z_b)^2/D_2^2}, \quad (21)$$

where z_t and z_b are the depths at the top and bottom of the cell, D_1 is the vertical scale of the outflow component of the flow, D_2 is the vertical scale of the inflow component, and the coefficient β is chosen so that no vertical flows through

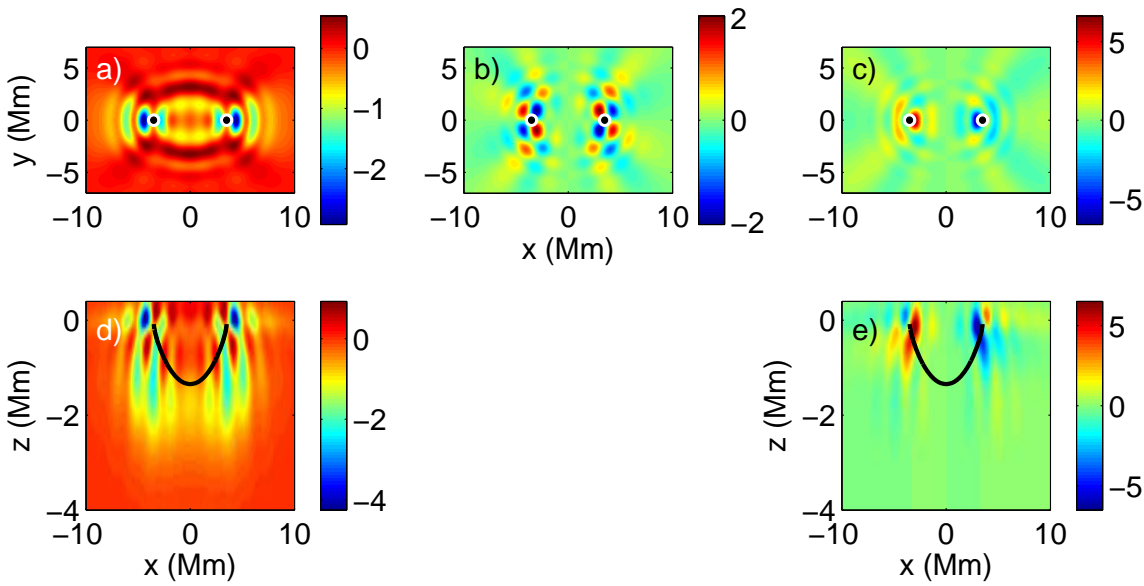


Fig. 1 Slices through an example of the sensitivity of a p_1 travel-time difference to local flows. Panels (a), (b), and (c) are horizontal slices, at the photosphere, through the kernels K_x , K_y , and K_z respectively. The symmetries of these three are different. The kernel K_x is symmetric in both x and y . The kernel K_y is symmetric in x and anti-symmetric for y . The kernel K_z is anti-symmetric x and symmetric in y . Because of these symmetries, only K_x has a non-zero total integral, as a result the travel-time difference $\delta\tau(\mathbf{x}_1, \mathbf{x}_2)$ is not sensitive (at first order) to uniform vertical flows or uniform flows in the cross-ray path direction. Panel (d) shows a slice through K_x at $y = 0$. The heavy black line shows the ray path. Notice that the p_1 mode structure is seen in depth. Panel (e) shows a slice through K_z at $y = 0$, again with the ray path shown as the heavy black line. By symmetry, the kernel K_y is zero at $y = 0$. In all panels the units are $\text{s Mm}^{-3}/(\text{km/s})$.

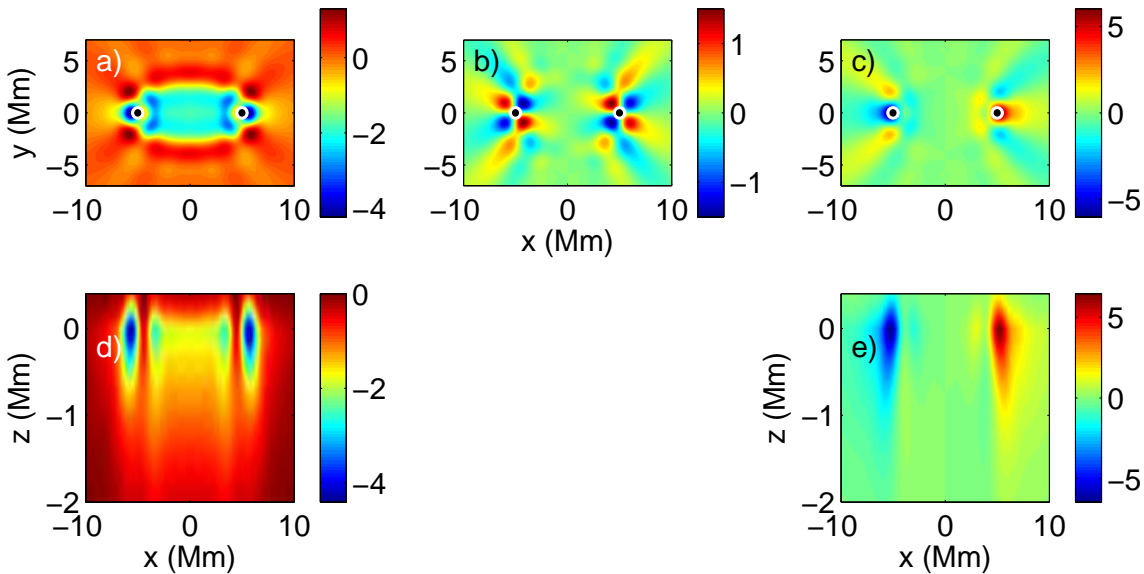


Fig. 2 Slices through the sensitivity of a f -mode travel time to local flows. Panels (a), (b), and (c) are horizontal slices, at the photosphere, through the kernels K_x , K_y , and K_z respectively. Panel (d) shows a slice through K_x at $y = 0$. Panel (e) shows a slice through K_z at $y = 0$. By symmetry, the kernel K_y is zero at $y = 0$. In all panels the units are $\text{s Mm}^{-3}/(\text{km/s})$.

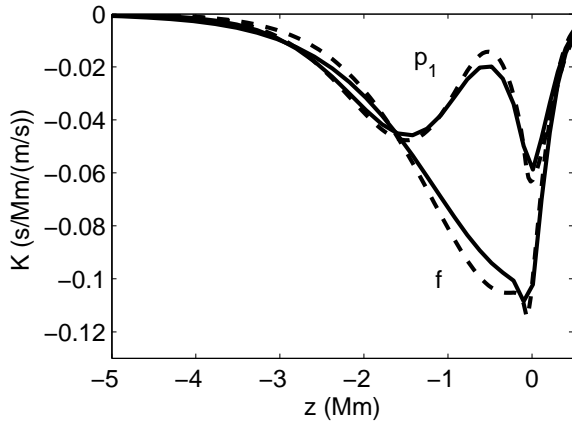


Fig. 3 Horizontal integrals of the K_x kernels for the p_1 and f cases (solid lines) shown in figures 1 and 2. Also shown are scaled kinetic energy densities (dashed lines) for the modes at the dominant wavenumber.

the cell are required by mass conservation. The depth dependence, $n(z)$, of the vertical flow we then choose so that the flow satisfies mass conservation

$$\partial_z [\rho_0(z)n(z)] = \rho_0(z)h(z), \quad (22)$$

with the upper boundary condition $n(z) = 0$ at $z = z_t$ where z_t is the top of the cellular flow.

We consider two models. Both have $(L, k) = (20 \text{ Mm}, 0.18 \text{ Mm}^{-1})$. Model A has $(z_t, z_b, D_1, D_2) = (0.2, -8, 8, 1) \text{ Mm}$ and model B has $(z_t, z_b, D_1, D_2) = (0.2, -2, 4, 0.5) \text{ Mm}$. In both cases we choose the amplitude a so that the maximum radial flow speed is 100 m s^{-1} . Model A represents a deep flow that has very little vertical variation near the photosphere. Model B represents a shallow flow. The radial and vertical flows for these two models are shown in figure 4.

For both models we compute the travel-time differences $\delta\tau(\mathbf{x}_1, \mathbf{x}_2)$ with $(\mathbf{x}_1, \mathbf{x}_2) = (x - \Delta/2, x + \Delta/2)\hat{\mathbf{x}}$, where Δ is the travel distance and $\hat{\mathbf{x}}$ is the unit vector in the x direction. For the ray-approximation travel times we use equation (15) from Kosovichev & Duvall (1997) with ray paths computed according to equation (11) of that paper, for the travel distance $\Delta = 7 \text{ Mm}$ (the same distance as for the kernels shown in Figure 1). We compute Born approximation travel-time shifts for the p -mode case described in §3.1.

Figure 5 shows the ray and Born approximation travel-time differences for model A, the deep cellular flow. The two approximations give travel-time shifts that are similar to within about two seconds. In the Born approximation, the contribution of \hat{z} component of the flow is about 5% of the contributions from the x component of the flow and the contribution from the \hat{y} component of the flow contributes less than one percent of the signal. We note here that we have used, in the ray approximation, only a single ray at 4.5 mHz (this is the frequency where the wavefield has maximum power). It may be that by taking a weighted average of many ray travel times, the ray approximation could

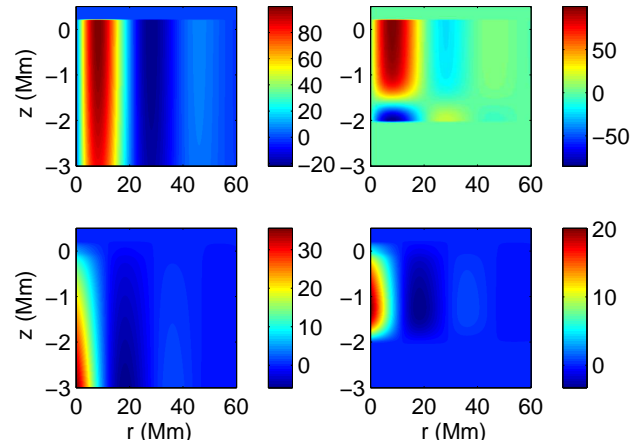


Fig. 4 Radial (top panels) and vertical (bottom panels) flows for model A (left column) and model B (right column). The units of the color scales are m/s. The axis of symmetry of the cellular flow is $r = 0$ and the photosphere is at $z = 0$. Upflows correspond to positive values of the vertical velocity.

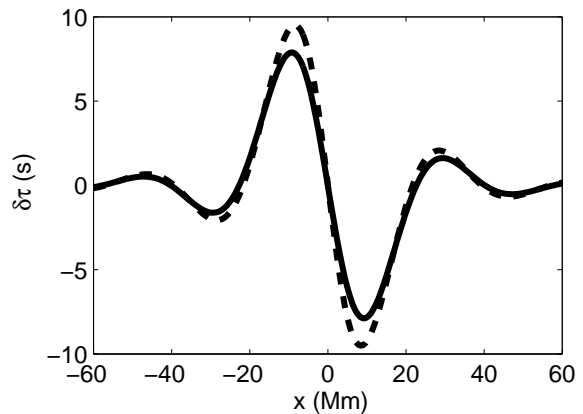


Fig. 5 Travel-time differences in the ray approximation (dashed line) and Born approximation (solid line) for model A “deep flow”. For this particular flow, the maximum difference between the two approximations is 2 s, about 25%.

be brought into agreement with the Born approximation. A study of this procedure is beyond the scope of this simple example.

Figure 6 shows the ray and Born approximation travel-time differences for model B, the shallow flow. For this case, the ray and Born approximations give substantially different results. The main cause of this difference is that the ray approximation is not sensitive to flows that are below the lower turning point of the ray, while in the Born approximation the sensitivity extends below the lower turning point. In this particular example, the strong counter-flow is sensed in the Born approximation, but not in the ray approximation.

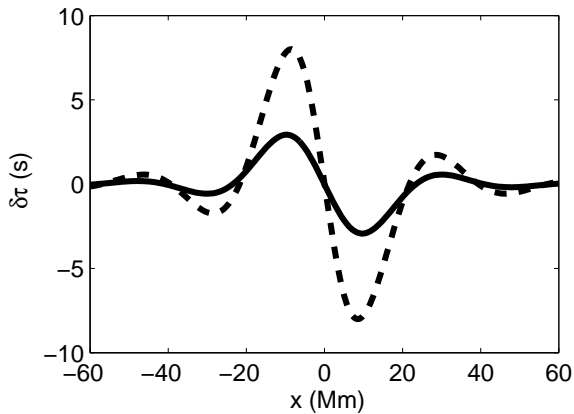


Fig. 6 Comparison between the ray approximation (dashed line) and Born approximation (solid line) for travel-time differences caused by the model B “shallow flow”. For this flow, the Born approximation and the ray approximation give travel-time shifts that differ by up to five seconds.

5 Discussion

We employed the Born approximation to obtain the three-dimensional sensitivity of time-distance measurements to advection by local flows. In this paper we addressed the important question of time-independent mass flows. We have shown that for horizontally uniform flows the depth dependence of the sensitivity of travel times is given approximately by the kinetic energy density of the mode which contributes most to the travel times.

For simple cylindrically symmetric models of supergranulation-scale convection cells we showed that the Born and ray approximations can give results that are substantially different when the flow varies in the depth range just below the lower turning point of the ray. This suggests that for inversions of supergranulation-scale flows it may be important to use kernels based on the Born approximation rather than the ray approximation.

In the future, a number of improvements could be implemented: inclusion of modes above the acoustic cutoff frequency, taking spherical geometry into account, and treatment of time-dependent flows.

Acknowledgements. The work of ACB was supported by NASA contracts NNH04CC05C and NNH06CD84C. It is planned to make this kernel calculation code available through the HELAS Network.

References

- Birch, A. C., Kosovichev, A. G. & Duvall, T. L., Jr.: 2004 ApJ 608, 580
 Birch, A. C. & Felder, G.: 2004, ApJ 616, 1261
 Birch, A. C. & Kosovichev, A. G.: 2000 Sol. Phys. 192, 193
 Christensen-Dalsgaard, J. & others 1996: Science 272, 1286
 Couvidat, S., Birch, A. C., Kosovichev, A. G.: 2006, ApJ 640, 516
 Duvall, T. L., Jr, Jefferies, S. M, Harvery, J. W., & Pomerantz, M. A.: 1993, Nature 362, 430

- Gizon, L. & Birch, A. C.: 2002, ApJ 571, 966
 Gizon, L., Duvall, T.L., Jr. & Larsen, R.M. 2000: JApA 21, 339
 Gizon, L., Duvall, T.L., Jr.: 2000b, Sol. Phys. 192, 177
 Jackiewicz, J., Gizon, L., Birch, A. C.: 2006, in Proc SOHO 18, ESA SP-624
 Kosovichev, A. G. & Duvall, Jr., T. L. 1997: “Acoustic tomography of solar convective flows and structures”, in: SCORE’96: Solar Convection and Oscillations and their Relationship, 241
 Lynden-Bell, D. & Ostriker, J. P. 1967: MNRAS 136, 293
 Zhao, J., Kosovichev, A.G., Duvall, T. L., Jr.: 2001, ApJ 557, 384
 Zhao, J., Kosovichev, A.G.: 2003, ApJ 591, 446
 Zhao, J., Kosovichev, A.G., Duvall, T. L., Jr.: 2004, ApJ 607, L135